Removing Solar Radiative Effect from the VIIRS M12 Band at 3.7 μm for Daytime Sea Surface Temperature Retrievals

QUANHUA LIU

NOAA/NESDIS/STAR, and Earth System Science Interdisciplinary Center, University of Maryland, College Park, College Park, Maryland

ALEXANDER IGNATOV AND FUZHONG WENG

NOAA/NESDIS/STAR, College Park, Maryland

XINGMING LIANG

Cooperative Institute for Research in the Atmosphere, Colorado State University, Fort Collins, Colorado

(Manuscript received 13 February 2014, in final form 27 June 2014)

ABSTRACT

Operational sea surface temperature (SST) retrieval algorithms are stratified into nighttime and daytime. The nighttime algorithm uses two split-window Visible Infrared Imaging Radiometer Suite (VIIRS) bands—M15 and M16, centered at ~11 and ~12 μm, respectively—and a shortwave infrared band—M12, centered at ~3.7 μm. The M12 is most transparent and critical for accurate SST retrievals. However, it is not used during the daytime because of contamination by solar radiation, which is reflected by the ocean surface and scattered by atmospheric aerosols. As a result, daytime VIIRS SST and cloud mask products and applications are degraded and inconsistent with their nighttime counterparts. This study proposes a method to remove the solar contamination from the VIIRS M12 based on theoretical radiative transfer model analyses. The method uses either of the two VIIRS shortwave bands, centered at 1.6 μm (M10) or 2.25 μm (M11), to correct for the effect of solar reflectance in M12. Subsequently, the corrected daytime brightness temperature in M12 can be used as input into nighttime cloud mask and SST algorithms. Preliminary comparisons with the European Centre for Medium-Range Weather Forecasts (ECMWF) SST analysis suggest that the daytime SST products can be improved and potentially reconciled with the nighttime SST product. However, more substantial case studies and assessments using different SST products are required before the transition of this research work into operational products.

1. Introduction

Sea surface temperature (SST) is critically important to characterize air–sea interaction, global water cycle, oceanic and atmospheric circulation and forecasting, climate, fisheries, tropical cyclogenesis, sea fog and sea-breeze formation, and for many other applications (Reynolds et al. 2007). Because of its extreme importance, SST was identified as one of the two priority environmental data records (EDRs), derived from the Visible Infrared Imager Radiometer Suite (VIIRS) on board the *Suomi National Polar-Orbiting Partnership* (*Suomi-NPP*).

VIIRS moderate-resolution (M) bands, centered at 3.75 (M12), 10.76 (M15), and 12.01 (M16) μm (Liu et al. 2012), are used for accurate SST mapping and retrievals. They have a spatial resolution of 750 m at nadir and 1600 m at the end of scan, and a wide scan that provides global coverage twice daily. Current operational SST retrieval algorithms are stratified into nighttime and daytime (Baker 2011). The nighttime algorithm uses two split-window bands, M15 and M16, and a shortwave infrared band, M12. During the daytime, band M12 is not used because of contamination by solar radiation. In a sun-glint region (e.g., for glint angles less than 10°), the solar radiation may increase the M12 radiance by 30% or more, and the corresponding M12 brightness

Corresponding author address: Quanhua Liu, ESSIC, University of Maryland, NOAA/NESDIS/Center for Satellite Applications and Research, College Park, 5830 University Research Court, College Park, MD 20740-3822.
E-mail: quanhua.liu@noaa.gov

DOI: 10.1175/JTECH-D-14-00051.1

temperature (BT) by more than 10 K (Liang et al. 2010). Daytime cloud detection is more robust than nighttime with visible and near-infrared bands. Without M12, the cloud masking is degraded, and SST retrieval accuracy will be degraded and inconsistent with their nighttime counterparts. The VIIRS SST is monitored daily at the National Oceanic and Atmospheric Administration (NOAA) using the SST Quality Monitor (SQUAM; www.star.nesdis.noaa.gov/sod/sst/squam/) system (Dash et al. 2010). The Monitoring of IR Clear-Sky Radiances over Oceans for SST (MICROS; www.star.nesdis.noaa.gov/sod/sst/micros/) is another web-based near-real-time system developed at NOAA that monitors corresponding Community Radiative Transfer Model (CRTM) model minus observation (M − O) biases and corresponding SST differences over the global ocean (Liang and Ignatov 2011). Data in MICROS suggest that global mean M − O biases in VIIRS M12 [and their corresponding standard deviations (STDs)] are −0.01 K (0.46 K) at night and −1.26 K (1.44 K) during the daytime (example numbers are for 11 February 2013, also representative for other days). As a result, the corresponding VIIRS SST biases (STDs) for "VIIRS SST minus Reynolds SST" are 0.16 K (0.48 K) at night and 0.47 K (0.59 K) during the daytime. Part of the increased daytime STD comes from the larger diurnal variability of the diurnal thermocline, but a larger part is due to the transparent M12 not being used in daytime SST retrievals. Zavody et al. (1998) have proposed a method for calibrating the second Along-Track Scanning Radiometer's (ATSR-2) 1.6-μm channel using simultaneous measurements made in the 3.7-μm channel in sun glint. Saharan dust is known to affect SST, and also significantly scatter solar radiation in the 3.7-μm band. The Saharan dust index (SDI) algorithm was proposed by Merchant et al. (2006) to correct SST derived from the Spinning Enhanced Visible and Infrared Imager for the effects of Saharan dust. The SDI uses the 3.7-μm band and therefore is used only at night now. Correcting the 3.7-μm band for solar reflectance can extend the SDI applications to daytime data. Subsequently, SDI can be potentially used with the VIIRS data to correct SST for aerosol effect.

In this paper, the VIIRS SST algorithm is briefly described in section 2. In section 3, we apply radiative transfer equations and derive a correction algorithm for removing solar contamination from the VIIRS M12 band based on reflectance measured in either VIIRS band M10 or M11. The algorithm is very simple and, once tested on larger globally representative data set, can be implemented operationally. Results are discussed in section 4. The summary and conclusion are given in section 5.

2. VIIRS SST algorithm

The VIIRS SST regression algorithms documented in Baker (2011) are the nonlinear multichannel SSTs (Walton et al. 1998; Petrenko et al. 2011). The nighttime SST algorithm uses the VIIRS M12 brightness temperature at 3.7 μm ($T_{3.7}$), M15 at 11 μm (T_{11}), and M16 at 12 μm (T_{12}), and is expressed as

$$\mathrm{SST} = a_0 + a_1 \times T_{11} + a_2 \times (T_{3.7} - T_{12}) \times T_{\mathrm{ref}} + a_3 \times (\sec\theta_{\mathrm{sat}} - 1). \quad (1)$$

Here, a_i are regression coefficients and θ_{sat} is the satellite view zenith angle at the surface. The daytime algorithm is expressed as

$$\mathrm{SST} = a_0 + a_1 \times T_{11} + a_2 \times (T_{11} - T_{12}) \times T_{\mathrm{ref}} + a_3 \times (T_{11} - T_{12}) \times (\sec\theta_{\mathrm{sat}} - 1). \quad (2)$$

The first-guess SST T_{ref} comes from either numerical weather prediction or analysis fields. There are two sets of fitting coefficients—one for dry conditions, $(T_{11} - T_{12}) < 0.6$ K, and the other for moist conditions, $(T_{11} - T_{12}) > 1$ K. For the intermediate cases, the operational algorithm linearly interpolates between the dry and moist SSTs. In this study, we have used regression coefficients directly from the *Suomi-NPP*/Joint Polar Satellite System (JPSS) operational system interface data processing segment (IDPS). Note that the IDPS coefficients were calculated prelaunch using Moderate Resolution Atmospheric Transmission (MODTRAN) radiative transfer simulations and therefore may result in offset (biases). However, the IDPS SST algorithm is expected to adequately capture the SST variability (STD). Recently, Petrenko et al. (2014) derived the regression coefficients and achieves a better accuracy.

The instrumental noise for M12, M15, and M16 is low. At a temperature of 300 K, the noise equivalent temperature differences NEΔT at the VIIRS baseline are 0.065, 0.038, and 0.07 K for M12, M15, and M16, respectively. The M12 is less affected by atmosphere and its NEΔT is between M15 and M16. VIIRS postlaunch performance is found to be better than the prelaunch specifications (Liu et al. 2012).

3. Removing solar contamination in M12

The VIIRS M12 band is centered at the wavelength of 3.75 μm. Over clear open ocean, VIIRS M12-measured radiance during the daytime is mainly composed of thermal emission and surface-reflected solar radiation. The VIIRS M10- and M11-measured radiance is dominant from the surface-reflected solar radiation, and the

thermal contribution is negligible. Therefore, we can use VIIRS M10 or M11 to remove the solar component from the M12 measurement. The SST algorithm is only applied under clear-sky conditions. Therefore, this study focuses on clear-sky conditions. As a first step, we concentrate on open-ocean cases where the aerosol optical depth is typically <0.1 and the aerosol effect is small in M10, M11, and M12. Neglecting scattering on aerosols, radiance at the top of the atmosphere (TOA) for M12 can be written as

$$R_{3.7} = \tau_{3.7}(\theta_{\rm sat})[\epsilon B(T_s) + (1-\varepsilon)R_{\rm atm\_d}] + R_{\rm atm\_u} + F_{3.7}\cos(\theta_{\rm sun})\tau_{3.7}(\theta_{\rm sat})\tau_{3.7}(\theta_{\rm sun})\rho_{3.7}. \quad (3)$$

Here, ε is the surface emissivity, τ is the transmittance from the top of the atmosphere to the surface, and ρ is surface bidirectional reflectance distribution function (BRDF), which depends upon the solar zenith angle $\theta_{\rm sun}$, satellite view zenith angle $\theta_{\rm sat}$, and their relative azimuth. On the right side of Eq. (3), the first term is the TOA radiance contributed by surface-emitted radiation and by the atmospheric downwelling radiation ($R_{\rm atm\_d}$) reflected from the surface. The second term is the upwelling atmospheric radiation ($R_{\rm atm\_u}$), and the third term is BRDF-reflected solar radiation.

The thermal emission in the shortwave infrared bands, M10 at 1.6 μm and M11 at 2.25 μm, is negligible and therefore the radiative transfer equation in those bands can be expressed as

$$R_\lambda = F_\lambda \cos(\theta_{\rm sun})\tau_\lambda(\theta_{\rm sat})\tau_\lambda(\theta_{\rm sun})\rho_\lambda. \quad (4)$$

Here, λ indicates band, M10 or M11. Note that the molecular (Rayleigh) optical depths in M10 and M11 are very small (only about 0.5% and 0.1%, respectively, of those in band M1 at 0.41 μm). For VIIRS, the M10 reflectance is typically less than 0.1% when the BRDF contribution is small (i.e., outside the sun glint), and the M11 reflectance is even smaller. Since the form of the BRDF-reflected solar radiation for M12, M11, and M10 is the same, one can use M10 or M11 radiance to predict solar radiation in M12. Using Eq. (4), the solar contamination in M12 can be expressed as

$$F_{3.7}\cos(\theta_{\rm sun})\tau_{3.7}(\theta_{\rm sat})\tau_{3.7}(\theta_{\rm sun})\rho_{3.7} = R_\lambda \frac{F_{3.7}\tau_{3.7}(\theta_{\rm sat})\tau_{3.7}(\theta_{\rm sun})\rho_{3.7}}{F_\lambda\tau_\lambda(\theta_{\rm sat})\tau_\lambda(\theta_{\rm sun})\rho_\lambda}. \quad (5)$$

The solar spectral irradiances $F_{3.7}$ and F_λ are known constants, and the total transmittances for the window channels are mainly functions of the column water vapor in the atmosphere. Note that Eq. (5) uses a ratio of total transmittances, which should minimize the sensitivity to small uncertainties (~5%) in the column water vapor and temperature profiles possibly present in the weather forecast data. The atmospheric transmittances for M10, M11, and M12 can be directly computed from the CRTM (Liu and Weng 2006) and parameterized as lookup tables. In this study, we apply the CRTM to compute the nadir optical depth for a tropical atmospheric profile that is scaled to produce a total column water vapor ranging from 5 to 70 mm. The optical depths are stored in a lookup table and used to compute transmittance at a satellite view zenith and sun zenith angles.

The most widely used BRDF model is a local facet model (Fresnel reflection Γ) with a weight depending on surface roughness slope distribution (Torrance and Sparrow 1976; Liu et al. 1998). The BRDF may be written as

$$\rho_\lambda = \Gamma(\lambda, \theta_{\rm local})\text{Weight}. \quad (6)$$

The $\theta_{\rm local}$ is the zenith angle at a local facet that is computed from incoming (sun) and outgoing (satellite) directions. Note that the Weight is actually unknown. Based on their sun-glint measurements, Cox and Munk (1954) suggested parameterizing the Gaussian distribution of a surface slope as a function of a wind speed. This approximation is the main source of error in the BRDF model. Also, the instantaneous wind speed may not be sufficiently accurate or complete to predict the surface roughness, which also depends on wind history (i.e., developing vs developed wind) and surface stability (Bréon and Henriot 2006; Liang et al. 2010). Fortuitously, the Weight only very weakly depends on wavelength and nearly cancels out in calculating the ratio of the BRDFs in Eq. (5). As a result, Eq. (5) can be rewritten as

$$F_{3.7}\cos(\theta_{\rm sun})\tau_{3.7}(\theta_{\rm sat})\tau_{3.7}(\theta_{\rm sun})\rho_{3.7} = R_\lambda \frac{F_{3.7}\tau_{3.7}(\theta_{\rm sat})\tau_{3.7}(\theta_{\rm sun})\Gamma(3.7,\theta_{\rm local})}{F_\lambda\tau_\lambda(\theta_{\rm sat})\tau_\lambda(\theta_{\rm sun})\Gamma(\lambda,\theta_{\rm local.})}. \quad (7)$$

The Fresnel reflection can be written as

$$\Gamma = \frac{1}{2}(r_v + r_h),$$

$$= \frac{1}{2}\left(\left|\frac{\sigma\cos\theta - \sqrt{\sigma - \sin^2\theta}}{\sigma\cos\theta + \sqrt{\sigma - \sin^2\theta}}\right|^2 + \left|\frac{\cos\theta - \sqrt{\sigma - \sin^2\theta}}{\cos\theta + \sqrt{\sigma - \sin^2\theta}}\right|^2\right). \quad (8)$$

For high wind speeds, foam should be considered, too. This study focuses on low and moderate wind speeds

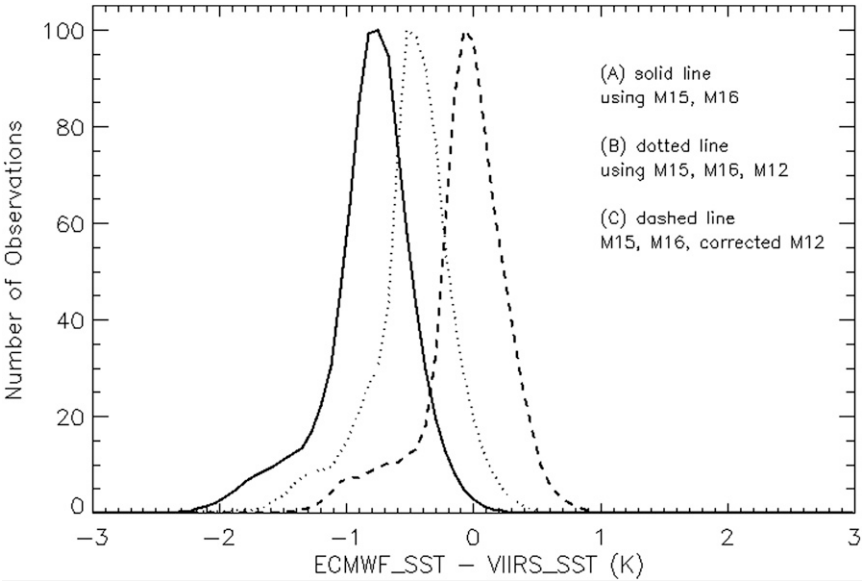

FIG. 1. Histogram of SST difference between ECMWF skin SST analysis and VIIRS SST: solid line for algorithm A, dotted line for algorithm B, and dashed line for algorithm C. The biases (STDs) are −0.77 (0.35), −0.37 (0.40), and −0.07 K (0.35 K) for algorithms A, B, and C, respectively. The number of data points is $N = 267\,006$.

only. Therefore, the corrected M12 radiance may be written as

$$R_{3.7}^{c} = R_{3.7} - F_{3.7}\cos(\theta_{\text{sun}})\tau_{3.7}(\theta_{\text{sat}})\tau_{3.7}(\theta_{\text{sun}})\rho_{3.7} = R_{3.7} - R_{\text{corr}}(\lambda)\ldots \quad (9)$$

The correction term is only Eq. (7),

$$R_{\text{corr}}(\lambda) = R_{\lambda}\frac{F_{3.7}\tau_{3.7}(\theta_{\text{sat}})\tau_{3.7}(\theta_{\text{sun}})\Gamma(3.7,\theta_{\text{local}})}{F_{\lambda}\tau_{\lambda}(\theta_{\text{sat}})\tau_{\lambda}(\theta_{\text{sun}})\Gamma(\lambda,\theta_{\text{local}})}. \quad (10)$$

The correction term depends only on the column water vapor, whereas the wind speed term in the BRDF completely cancels out. In these analyses, we use the column water vapor from the European Centre for Medium-Range Weather Forecasts (ECMWF) 6-h analysis. Also, we have opted to use the reflective spectral band M10 to predict solar reflectance in M12 because its signal-to-noise ratio is more than an order of magnitude larger than that of M11. Equations (9) and (10) will be used to remove solar contamination in this study.

4. Results

Several clear-sky uniform oceanic areas were selected based on the VIIRS M2, M4, and M5 true-color images. Once a rectangular clear-sky area was identified, neither cloud masking nor quality control was applied. VIIRS M12 daytime ocean images were separately analyzed for several conditions: area most affected by the BRDF (sun glint), least affected by BRDF (outside sun glint), and a case in between. Another case near the equator is also investigated.

We first investigated an easy case, the VIIRS M12 BT image over a clear-sky ocean near Mexico. The BRDF effect is very small here, as the sun-glint angle is larger than 30° and the sea surface is calm (wind speed is $\sim 3.5\,\text{m s}^{-1}$). Figure 1 checks the sensitivity of the VIIRS SST to the algorithm used: algorithm A is the standard daytime VIIRS SST product derived from bands M15 and M16; algorithm B is a result of the application of the nighttime algorithm to daytime BTs in bands M15, M16, and M12; and algorithm C is the same as algorithm B, except M12 has been now corrected for solar contamination using Eqs. (9) and (10). Biases using the algorithms A, B, and C are −0.77, −0.37, and −0.07 K, respectively. The root-mean-square (RMS) errors are 0.84, 0.54, and 0.36 K, respectively. Prior to correcting M12, the nighttime algorithm B shows a larger STD (0.40 K) than the daytime algorithm A (0.35 K). This is expected, since solar reflectance outside the glint area is small but not negligible. However, when the M12 is corrected for (relatively small in this case) solar contamination, the nighttime algorithm C improves the STD (0.35 K) over algorithm B and makes it comparable with the operational split-window daytime algorithm A.

Figure 2a is another VIIRS M12 BT image over a clear-sky ocean near Australia, but the sun-glint angle is now less than 10° here and the surface wind speed is high, more than $7\,\text{m s}^{-1}$. The white area in Fig. 2a represents strong solar contamination in the glint area.

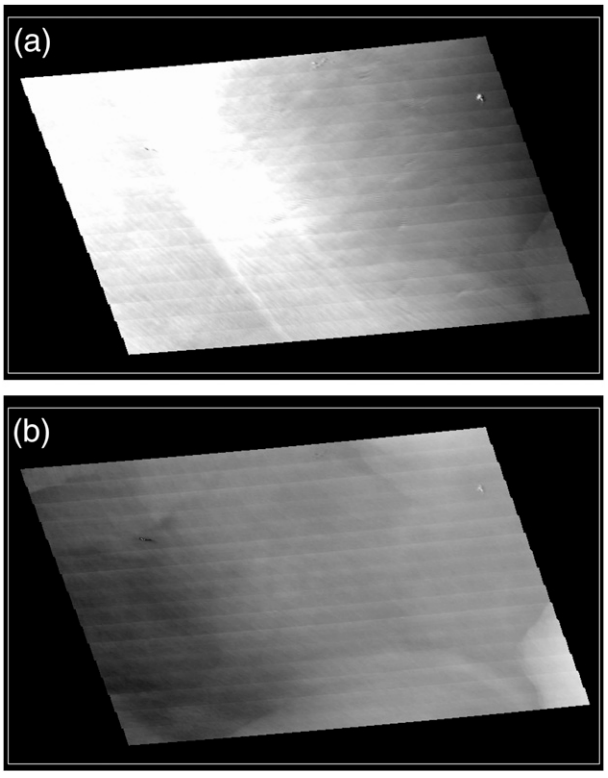

FIG. 2. (a) VIIRS BT image in M12 (301–307 K) over a clear-sky ocean near Australia at 0615 UTC 25 Jan 2013. The sun-glint angle is less than 10° and the ECMWF sea surface wind speed is $>7\,m\,s^{-1}$. (b) As in (a), but after solar radiation was removed using Eqs. (9) and (10). Note that grayscale is now from 292 to 298 K.

Note that the striping in the along-track direction displaying a periodic pattern comes from the fact that VIIRS uses 16 detectors for each M band and 32 detectors for each I band (Cao et al. 2013).

The M12 image is corrected using Eqs. (9) and (10), and plotted in Fig. 2b, which shows that the correction removed the most solar contamination. The small residual may be due to sea foam, a small error in the VIIRS band-to-band registration, and an aerosol effect that was not taken into account. The small residual striping caused by the significant difference among the 16 detectors' azimuth angles is irrelevant to the scope of this paper and will be discussed elsewhere. Figure 3 compares the three algorithms. Biases using the algorithms A, B, and C are −0.85, −10.24, and −0.76 K, respectively. The root-mean-square errors are 0.90, 0.10.36, and 0.81 K, respectively. Application of the nighttime algorithm to the corrected M12 has the smallest STD, suggesting that in the glint area during the daytime, the use of corrected M12 improves the accuracy of the SST product over the standard daytime M15- and M16-based algorithm.

We have analyzed another image near Australia (0628 UTC 4 February 2014) with a moderate solar contamination, somewhere in between the two cases shown in Figs. 1 and 3. Figure 4 compares the three algorithms. Biases using the algorithms A, B, and C are −1.28, −2.54, and −0.19 K, respectively. The RMS errors are 1.29, 2.56, and 0.23 K, respectively. The SST based on using the nighttime algorithm in conjunction with the corrected M12 shows the VIIRS SST closest to the ECMWF analysis, in an RMS sense. The skin temperature in the ECMWF analysis is close to a radiometric skin temperature because many infrared radiances are directly assimilated in the analysis and the infrared radiances measure radiometric skin temperature.

We also analyzed an image near the equator. The image located in Northeast Brazil is on 1 January 2013. Near the equator, the sun glint is stronger and the solar contamination is large. Figure 5 showed a similar comparison to that in Figs. 1, 3, and 4. Biases using the algorithms A, B, and C are −0.68, −7.27, and −0.16 K, respectively. The RMS errors are 0.28, 1.54, and 0.35 K, respectively.

5. Conclusions

This paper discusses the approach to remove solar contamination from the VIIRS M12 centered at 3.7 μm during the daytime. The corrected M12 radiance contains predominantly thermal radiation, so that the VIIRS nighttime SST algorithms can be applied to the daytime M12 data. The case studies analyzed here suggest that most solar contamination in M12 can be effectively removed using radiances in the reflective spectral band M10 or M11. We analyzed several case studies at different locations and observation times: the one least affected by BRDF, the one most strongly affected, and the one moderately affected. We also analyzed cases near the equator. We compared the SST algorithms against the surface skin temperature from the ECMWF analysis. Results suggest that using corrected M12 during the day has a potential to improve the retrieved SST.

Note that over clean and foam-free oceans, the M10 and M11 are mainly affected by solar radiation reflected from the surface and their emission signals are negligible. Therefore, one may use their reflectance to decide whether correction in M12 is needed. If the reflectance in M10/M11 is below a certain threshold (say, 0.1%), then M12 may be considered "uncontaminated" and no correction may be needed. Otherwise, the correction is required.

The method described in this study does not take into account the aerosol scattering and is only limited to the areas having small aerosol concentrations. Also, it does not consider sea foam and is limited to surface wind speeds less than $10\,m\,s^{-1}$. This algorithm may

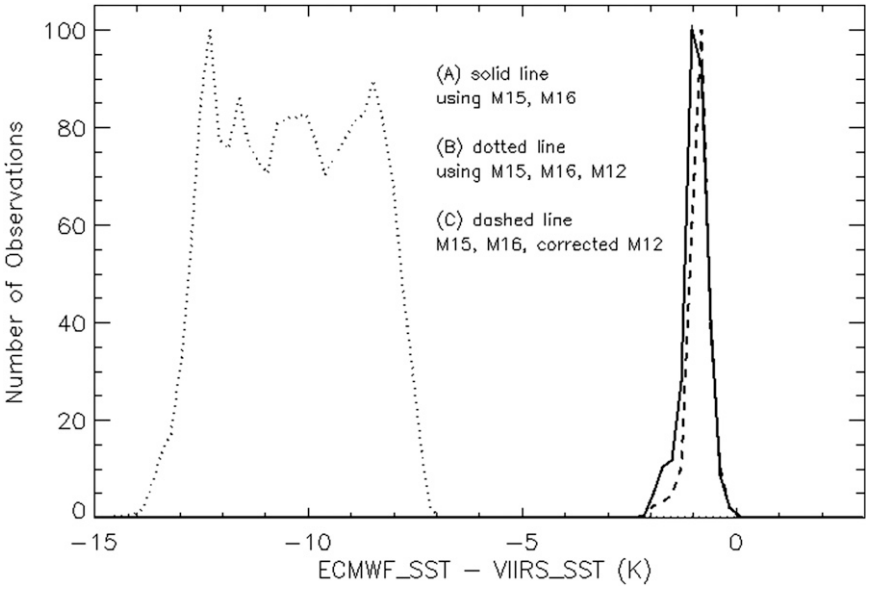

FIG. 3. As in Fig. 1, but for data near Australia at 0615 UTC 25 Jan 2013. The biases (STDs) are −0.85 (0.30) K, −10.24 (1.58) K, and −0.76 (0.27) K for algorithms A, B, and C, respectively. The number of data points is $N = 46\,330$.

be extended to aerosol-burdened cases using two reflectances from M10 and M11 to obtain information about aerosol optical depth and surface direct reflectance, simultaneously. Alternatively, data from global aerosol models such as the Goddard Chemistry Aerosol Radiation and Transport (GOCART) model or the Navy Aerosol Analysis and Prediction System (NAAPS) can be input into the CRTM to estimate solar radiation. Merchant et al. (2009) correct the contribution to brightness temperature in the Geostationary Operational Environmental Satellite (GOES) 3.9-mm channel from solar irradiance. Future works will include substantial

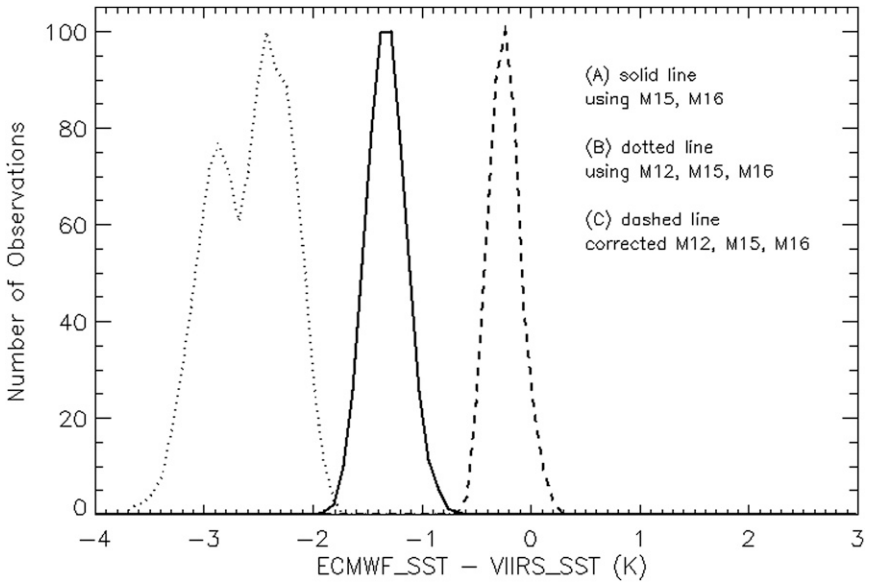

FIG. 4. As in Fig. 1, but for data near Australia at 0628 UTC 4 Feb 2013. The biases (STDs) are −1.28 (0.18) K, −2.54 (0.36) K, and −0.19 (0.14) K for algorithms A, B, and C, respectively. The total number of data points is $N = 12\,928$.

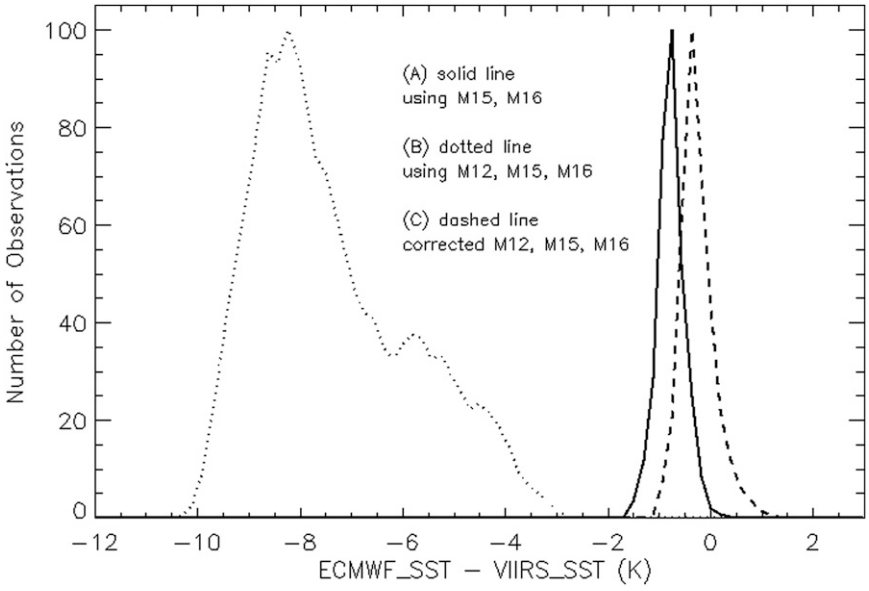

FIG. 5. As in Fig. 1, but for data near Brazil at 1621 UTC 1 Dec 2013. The biases (STDs) are −0.68 (0.28) K, −7.27 (1.54) K, and −0.16 (0.35) K for algorithms A, B, and C, respectively. The total number of data points is $N = 138\,850$.

case studies using different SST products over various locations and seasons. We will evaluate the performance of our algorithm against in situ SST measurements, including dedicated radiosondes and surface data acquired from NOAA Aerosols and Ocean Science Expeditions (AEROSE).

Acknowledgments. This work is supported by the Joint Center for Satellite Data Assimilation. Thanks to Boris Petrenko for providing the coefficients for the VIIRS IDPS SST algorithm. The views, opinions, and findings contained in this report are those of the authors and should not be construed as an official NOAA or U.S. government position, policy, or decision.

REFERENCES

Baker, N., 2011: Joint Polar Satellite System (JPSS) VIIRS sea surface temperature algorithm theoretical basis document (ATBD). ATBD, JPSS Ground Project Code 474, 474-00048, 62 pp. [Available online at http://www.star.nesdis.noaa.gov/jpss/documents/ATBD/474-00048_VIIRS_Sea-Surface-Temperature_ATBD_Rev-_20110422.pdf.]

Bréon, F. M., and N. Henriot, 2006: Spaceborne observations of ocean glint reflectance and modeling of wave slope distributions. *J. Geophys. Res.,* **111,** C06005, doi:10.1029/2005JC003343.

Cao, C., J. Xiong, S. Blonski, Q. Liu, S. Uprety, X. Shao, Y. Bai, and F. Weng, 2013: Suomi NPP VIIRS sensor data record verification, validation, and long-term performance monitoring. *J. Geophys. Res. Atmos.,* **118,** 11 664–11 678, doi:10.1002/2013JD020418.

Cox, C., and W. Munk, 1954: Statistics of the sea surface derived from sun glitter. *J. Mar. Res.,* **13,** 198–227.

Dash, P., A. Ignatov, Y. Kihai, and J. Sapper, 2010: The SST Quality Monitor (SQUAM). *J. Atmos. Oceanic Technol.,* **27,** 1899–1917, doi:10.1175/2010JTECHO756.1.

Liang, X., and A. Ignatov, 2011: Monitoring of IR Clear-Sky Radiances over Oceans for SST (MICROS). *J. Atmos. Oceanic Technol.,* **28,** 1228–1242, doi:10.1175/JTECH-D-10-05023.1.

——, ——, Y. Han, and H. Zhang, 2010: Validation and improvements of daytime CRTM performance using AVHRR IR 3.7 μm band. *13th Conf. on Atmospheric Radiation,* Portland, OR, Amer. Meteor. Soc., P2.3. [Available online at https://ams.confex.com/ams/13CldPhy13AtRad/techprogram/paper_170593.htm.]

Liu, Q., and F. Weng, 2006: Advanced doubling-adding method for radiative transfer in planetary atmosphere. *J. Atmos. Sci.,* **63,** 3459–3465, doi:10.1175/JAS3808.1.

——, C. Simmer, and E. Reprecht, 1998: Monte Carlo simulations of the microwave emissivity of sea surface. *J. Geophys. Res.,* **103,** 24 983–24 989, doi:10.1029/98JC01626.

——, C. Cao, and F. Weng, 2012: NPP VIIRS emissive band radiance calibration. *Earth Observing Systems XVII,* J. J. Butler, X. Xiong, and Xingfa Gu, Eds., International Society for Optical Engineering (SPIE Proceedings, Vol. 8510), 85101E, doi:10.1117/12.930201.

Merchant, C. J., O. Embury, P. Le Borgne, and B. Bellec, 2006: Saharan dust in nighttime thermal imagery: Detection and reduction of related biases in retrieved sea surface temperature. *Remote Sens. Environ.,* **104,** 15–30, doi:10.1016/j.rse.2006.03.007.

——, A. R. Harris, E. Maturi, O. Embury, S. N. MacCallum, J. Mittaz, and C. P. Old, 2009: Sea surface temperature estimation from the *Geostationary Operational Environmental Satellite-12* (*GOES-12*). *J. Atmos. Oceanic Technol.,* **26,** 570–581, doi:10.1175/2008JTECHO596.1.

Petrenko, B., A. Ignatov, N. Shabanov, and Y. Kihai, 2011: Development and evaluation of SST algorithms for GOES-R ABI using MSG SEVIRI as a proxy. *Remote Sens. Environ.,* **115,** 3647–3658, doi:10.1016/j.rse.2011.09.003.

——, ——, Y. Kihai, J. Stroup, and P. Dash, 2014: Evaluation and selection of SST regression algorithms for JPSS VIIRS. *J. Geophys. Res. Atmos.,* **119,** 4580–4599, doi:10.1002/2013JD020637.

Reynolds, R. W., T. M. Smith, C. Liu, D. B. Chelton, K. S. Casey, and M. G. Schlax, 2007: Daily high-resolution-blended analyses for sea surface temperature. *J. Climate,* **20,** 5473–5496, doi:10.1175/2007JCLI1824.1.

Torrance, K., and E. Sparrow, 1976: Theory for off-specular reflection from roughened surfaces. *J. Opt. Soc. Amer.,* **57,** 1105–1114, doi:10.1364/JOSA.57.001105.

Walton, C., W. Pichel, J. Sapper, and D. May, 1998: The development and operational application of nonlinear algorithms for the measurement of sea surface temperatures with the NOAA polar-orbiting environmental satellites. *J. Geophys. Res.,* **103,** 27 999–28 012, doi:10.1029/98JC02370.

Zavody, A. M., P. D. Watts, D. L. Smith, and C. T. Mutlow, 1998: A novel method for calibrating the ATSR-2 1.6-μm channel using simultaneous measurements made in the 3.7-μm channel in sun glint. *J. Atmos. Oceanic Technol.,* **15,** 1243–1252, doi:10.1175/1520-0426(1998)015<1243:ANMFCT>2.0.CO;2.